Self-collision Detection using Sphere Chains

Francisco A. Madera, Enrique Ayala, Francisco Moo-Mena
Facultad de Matematicas, Universidad Autonoma de Yucatan, Merida, Yucatan, Mexico

Keywords: Collision Detection, Human Animation, Approximation with Spheres.

Abstract: An algorithm to detect self-collisions in a human object is presented. We proposed to approximate the human object by spheres, which are placed inside the object mesh to fill the correspondent volume. We introduce the concept of sphere chain, a set of joined spheres which contains some regions of the human mesh. The object is approximated by several chains in the preprocessing stage to be prepared for the running stage to perform the collision detection.

1 INTRODUCTION

Self-collision refers to the collision of the primitives in the same object and it happens during the animation, when some regions of the object mesh are overlapped. To detect this kind of overlap helps to obtain an efficient animation cycle: animation, collision detection, collision response. Common collision detection methods involve two stages: the mesh preparation in a preprocessing stage, and the collision detection in the animation stage.

Objects can be approximated with basic primitives such as spheres, boxes, OBB (Oriented Bounding Box), among others. The construction of a hierarchy with Bounding Volumes (BV) can be performed using a top-down or a bottom-up approaches. The bottom-up approach has shown better results in the accuracy (Ericson, 2005). Rather than start with a triangle, we decided to start from a set of triangles that form a tubular shape and that can be bounded with a sphere.

Human movement is one of the most labor intensive tasks in computer graphics and animation applications: games, simulations, medicine, etc. We divide the human in five regions and bound each one with spheres. Regions have tubular (limbs) or non-tubular (torso) shapes. By joining the set of spheres of each region we can form a chain of spheres that covers part of the human mesh. As a result, we can perform the collision detection between the spheres of the chains independently of the other chains.

We pursuit to balance the throughput of the collision detection process, grouping the whole set of spheres of the mesh in smaller sets of spheres called chains. The division of the work of the collision detection makes to handle the process with less number of primitives in every part, the chains, independently of each other. We suggested to partition the mesh in tubular regions to form chains, taking advantage of the articulated object.

We can exploit the fact that the chain's collision detection are independent of the other chains to improve the time of the running stage in a parallel implementation. The sphere chains can be grouped in a hierarchy and have a BVH (Bounding Volume Hierarchy) constructed, but we decided to leave the sphere chains as they are, since there are few spheres. This implementation is created for the whole mesh with sphere chains ($\mathcal{M}_1$) and without sphere chains ($\mathcal{M}_2$) to compare their efficiency in sequential and in parallel implementations.

The contributions are as follows:

- The extension of a tubular sphere approximation to non-tubular regions to fill the human torso.
- The decomposition of a human object by chains of spheres.
- The comparison of the performance of the self-collision detection algorithm with and without chains.
- The parallel implementation of the collision detection algorithm.

The remain of the paper is organized as follows: In Section 2 previous work is presented, Section 3 details the sphere approximation for tubular and for non-tubular regions, in Section 4 the chain construction is described. The running stage is detailed in Section 5, and involves two processes: the sphere update, and

A. Madera F., Ayala E. and Moo-Mena F..
Self-collision Detection using Sphere Chains.
DOI: 10.5220/0005301603250331
In *Proceedings of the 10th International Conference on Computer Graphics Theory and Applications* (GRAPP-2015), pages 325-331
ISBN: 978-989-758-087-1

the overlapping test. Experimental results are performed in Section 6, and finally conclusion and further work are presented in Section 7.

2 PREVIOUS WORK

Collision detection in articulated objects have been investigated for years. Some methods focus on the segments of bones to build a rigid body geometry such as (Zhang et al., 2007) where an algorithm to perform self-collisions is proposed. It consists of one preprocessing step and two run-time steps: (1) preprocessed link-level bounding volume hierarchy (BVH) construction, (2) link-level spatial culling using Taylor models and a dynamic BVH and (3) exact contact determination using conservative advancement and temporal culling. This method requires the skeleton, the motion bound calculation, and the OBB hierarchy construction. Moreover, they construct Taylor models to improve the accuracy of the OBBs. Another work based on the same motion that considers rigid segments in articulated objects is found in (Kim et al., 2014). This method employs SSV (swept sphere volumes) to detect collisions and returns the first time of impact between the rigid bodies.

Even when rigid bodies can speed up the self-collision detection in articulated bodies, the information returned is the first contact point, so that for a mesh representation, a set of polygons is required. This manner, (Kavan et al., 2006) describe how to perform collision detection for models skinned with a spherical method. They suggested a procedure for refitting of bounding spheres for spherical blend skinning with sub-linear time complexity. The collision depends on the motion, the joint transformation matrices which requires the skeleton of the human. Our spheres are tighter than the ones used in this method, moreover our updating process is faster since it depends on the pivot polygons motion.

Spheres and ellipses are also utilized in (Müller and Chentanez, 2011), where a simulation particles are placed on a given visual mesh, which are connected to form a simulation mesh. The particles are driven by the simulation while the vertex positions are computed from the particle positions via skinning. Animated particles are used to attach the simulation mesh or as collision primitives. Similar to the method proposed in this work, they create spheres tangent to the surface particles (ellipsoids), so that ellipsoids are replaced by their circumspheres in the collision response process. We propose to create a sphere approximation filling the volume of the tubular shapes rather than bounding the polygons of the mesh.

The study of spheres aligned in a sequential order was suggested by Guibas et al (Guibas et al., 2002) and Ayala (Enrique Ayala, 2014). Guibas proposed to study deformable necklaces flexible chains of balls, called beads, in which only adjacent balls may intersect. Ayala et al. study the self-collision detection of a sequence of spheres with strong deformations using binary trees. These two last methods work with spheres disregarding the object mesh, so that considerations of the mesh must be done by using techniques of volume filling such as (Shier and Bourke, 2013) where a solid can be filled with basic primitives. In particular sphere packing has been investigated as a theoretical foundation and implemented in several applications such as radio surgical treatment planning (Teuber et al., 2013).

Another work of inspiration is the method proposed in (Weller and Zachmann, 2009), where data structure called the Inner Sphere Trees to fill the interior of the object with a set of non-overlapping volumes that approximate the object's volume is performed. Our work disregard the non-overlapping feature due to we pursuit the collision detection processing. Unlike that work, we do not test the penetration volume, but we handle less number of spheres. Every sphere is attached to its closed triangle similar to ours. However, this method is prepared for rigid bodies only.

Li et al. (Li et al., 2011) used a disk filled with rays to construct cages in the human body. Cages are utilized to deform the human during the skinning deformation. While we employ a disk, they employed several disks to form the cages with more memory usage. Zhu et al. (Zhu et al., 2013), define a torso cross-section to extract the geometric characteristics of human models for clothing design. The application is just for modeling, so that they did not regard the issues for animation and collisions.

3 SPHERE APPROXIMATION

A region $\mathcal{R}_i$ of the mesh consists of a set of polygons $\Delta = \{\Delta_0, \Delta_1, ..., \Delta_{n-1}\}$. A human mesh is divided in five regions as suggested in (Wang et al., 2014) and illustrated in Figure *1*. The regions are as follows: the left arm $\mathcal{R}_0$, the right arm $\mathcal{R}_1$, the left leg $\mathcal{R}_2$, the right leg $\mathcal{R}_3$, and the torso $\mathcal{R}_4$.

3.1 Tubular Regions

$\mathcal{R}_0$, $\mathcal{R}_1$, $\mathcal{R}_2$, and $\mathcal{R}_3$ are tubular regions that can be approximated by a set of spheres. Spheres created along the surface of the tubular object (represented

Figure 1: The human mesh is partitioned in five regions (left) and approximated with spheres (right).

by triangular meshes) are located in the center of the diameter of their corresponding region and they have the exact size as they collide with the surface. Thus, there are four approximated tubular regions: $\varphi(\mathcal{R}_0)$, $\varphi(\mathcal{R}_1)$, $\varphi(\mathcal{R}_2)$, $\varphi(\mathcal{R}_3)$.

We utilised the method proposed in (Madera et al., 2013) where the algorithm finds the shape defined by the base curve of the input object. A circumference is positioned in one of the ends of the tubular mesh, then, the circumference starts moving along the mesh looking for the best way to construct a sphere over its center. After a sphere is created, the circumference continues moving along the surface looking for the best places to create spheres.

3.2 Non-tubular Regions

The torso is approximated with spheres $\varphi(\mathcal{R}_4)$; in fact, we extent the method used for tubular objects explained above to non-tubular objects. We employ a disk filled with rays, which comes from the center of the disk and points outwards. The disk is placed on the bottom part of the torso and starts moving up along the torso with a displacement of δ units. During this motion, the ray-triangle intersection test is performed with the rays of the disk and the polygons of the object's mesh. The number of rays N_r is 80 and the disk traces the torso and determines the convenient locations to construct spheres. The information recorded is utilized to create spheres.

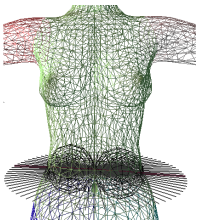

Figure 2: Two sequences of spheres vertically aligned to the y-axis due to the stand up pose is aligned to the y-axis.

A human torso is not a tubular-shaped object. This means that only one sphere is not a good approximation, two spheres per level (disk position) were employed instead, $N_s = 2$ (Figure 2). We partition the volumetric object in two sets, specifically the surrounding region obtained from the disk translation is divided in two parts (Figure 3). The surrounding region is formed by a set of polygons that collide with the rays of the disk. To calculate the accuracy of the sphere approximation, we tested the difference between the mesh bounded and the correspondent sphere. We call this measure F and it is computed for each vertex v_i of the surrounding region and indicates the difference between the radius of the sphere and the distance of its center and such a vertex: $F_i = \bigodot.r - \|\bigodot.c - v_i\|$.

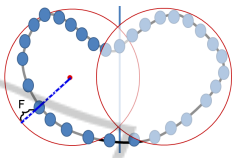

Figure 3: The surrounding region is divided in two parts and approximated with a sphere each.

Even when two or more spheres can have a better approximation than using only a sphere, spheres can be adjusted to improve their accuracy. The motion of the circumferences takes place in the plane formed by $\vec{\gamma}_0\vec{\gamma}_1$ towards the disk center direction (Figure 4). Doing this translation, the overlapping among the spheres is unavoidable, but this does not affect the accuracy. This is called the sphere adjustment process.

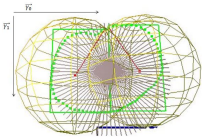

Figure 4: Spheres can be moved along the plane $\vec{\gamma}_0\vec{\gamma}_1$ towards the disk center direction.

We observe in Figure 4 that the set of vertices in green are partitioned in two parts, having bounded by a sphere each. Spheres are scaled down and moved towards each other in order to obtain more accurate approximation as depicted in Figure 5. This way, F is minimized and spheres become more accurate.

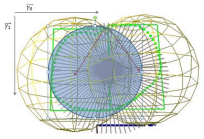

Figure 5: The left sphere can be scaled down to the size of the blue sphere.

Since the torso has an elliptical shape, we decided to use two vertical sequences of spheres to fill it. As

the spheres of the torso are arranged in two vertical sequences, we label the different sides as following: the left side spheres $\varphi(\mathcal{R}_4)_L$, the right side spheres $\varphi(\mathcal{R}_4)_R$, the top side spheres $\varphi(\mathcal{R}_4)_T$, and the down side spheres $\varphi(\mathcal{R}_4)_D$ as illustrated in Figure 6.

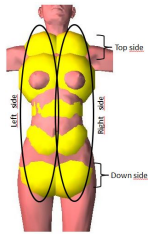

Figure 6: The left $\varphi(\mathcal{R}_4)_L$, right $\varphi(\mathcal{R}_4)_R$, top $\varphi(\mathcal{R}_4)_T$, and down $\varphi(\mathcal{R}_4)_D$ spheres of the torso.

We compare the accuracy of our spheres approximation method (φ_1) against the accuracy of the minimum enclosing ball algorithm (φ_2) proposed by Welz (Welzl, 1991). This comparison is performed with the F value. We first obtain a sphere from a set of vertices, and then we apply the adjustment process to increase the accuracy (φ_1').

4 CHAIN CONSTRUCTION

Tubular regions are approximated by a set of joined spheres that contains only a limb of the human. We proceeded to group the set of joined spheres for two limbs and therefore to create a chain of spheres. As we have four limbs, we take them in pairs, forming 6 chains. Note that the union of the spheres of two limbs includes some spheres of the torso.

Let ζ_i be the chain i formed by the union of the spheres of some regions, then we have the chains constructed in Table 1 and depicted in Figures 7 and 8.

Table 1: The six chains of the human mesh.

$\zeta_0 = \varphi(\mathcal{R}_0) \cup \varphi(\mathcal{R}_4)_L \cup \varphi(\mathcal{R}_2)$
$\zeta_1 = \varphi(\mathcal{R}_1) \cup \varphi(\mathcal{R}_4)_R \cup \varphi(\mathcal{R}_3)$
$\zeta_2 = \varphi(\mathcal{R}_0) \cup \varphi(\mathcal{R}_4)_T \cup \varphi(\mathcal{R}_1)$
$\zeta_3 = \varphi(\mathcal{R}_2) \cup \varphi(\mathcal{R}_4)_D \cup \varphi(\mathcal{R}_3)$
$\zeta_4 = \varphi(\mathcal{R}_0) \cup \varphi(\mathcal{R}_4)_T \cup \varphi(\mathcal{R}_4)_R + \varphi(\mathcal{R}_3)$
$\zeta_5 = \varphi(\mathcal{R}_1) \cup \varphi(\mathcal{R}_4)_T \cup \varphi(\mathcal{R}_4)_L + \varphi(\mathcal{R}_2)$

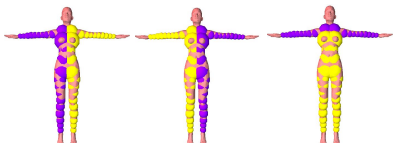

Figure 7: Spheres of chains 0,1,2 in purple.

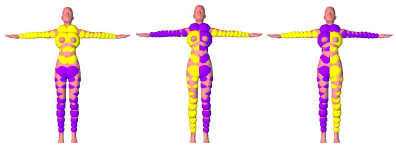

Figure 8: Spheres of chains 3,4,5 in purple.

Some spheres belong to more than one chain, due to a limb is connected to the other three limbs. We based our collision detection algorithm in the sphere overlap test using a brute force rather than using a BVH. In the future, when creating the Narrow Phase, finer approximation can be done by taking the spheres as root nodes and creating their child nodes to bound the polygons of the surrounding region.

5 THE RUNNING STAGE

In the running stage, the human is animated, the self-collision detection is called in every frame and the spheres are refitted.

5.1 Sphere Update

Sphere contains a set of polygons, that is, a polygon is assigned to the sphere closest to it. This way, $\Delta_i \in \bigodot_j$ if and only if $\| \bigodot_j .c - \Delta_i \| \leq \| \bigodot_k .c - \Delta_i \|$, $\forall k \neq j$. We call this set of polygons the surrounding region of sphere j (Figure 9).

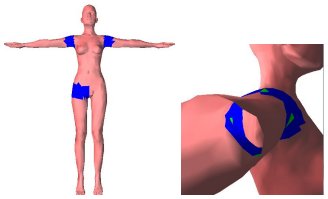

Figure 9: Surrounding regions of three spheres (left) and the four pivot polygons of a surrounding region(right).

We implemented an animation using the morphing method. Some poses are taken as basis of the frames and a quadric Bézier interpolation is applied between such poses to obtain smooth deformations.

During the human motion, spheres are updated to follow the mesh deformation. We use four polygons for each surrounding region which indicates the motion to be followed (Figure 9, right). In every frame, polygons of the mesh are moved, so that $\bigodot_j .c += \frac{1}{4}(\Delta_r + \Delta_s + \Delta_t + \Delta_u)$, where $\Delta_r, \Delta_s, \Delta_t, \Delta_u \in \bigodot_j^{\Delta}$. Thus, the new position of $\bigodot_j$ is the average of the new positions of its pivot polygons (Figure 10). The radius is also re-calculated taking the average of

the distances from the center of the sphere to the pivot polygons.

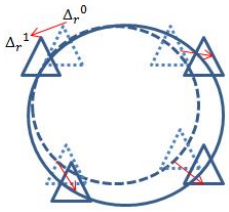

Figure 10: Sphere center is updated with the centroid of its four pivot polygons. Sphere marked with dotted lines is deformed to the sphere marked with solid lines.

An improvement would be to have more pivot polygons to refit the sphere size, but more expensive operations are demanded.

5.2 Overlapping Test

An application to use the approximation is presented: the collision detection algorithm. In this work we only implemented the brute force approach in sequential and parallel versions. The construction of the BVH demands parent and children nodes, that obviously increase the number of spheres and therefore a benefit to a parallel implementation.

Self-collision is performed by checking an overlap between spheres in each chain. This is a broad phase collision detection which returns the pairs of spheres colliding and therefore the surrounding regions involved. An overlap between spheres $\bigodot_A$ and $\bigodot_B$ occurs if $(\| \bigodot_A.c - \bigodot_B.c \|_2)^2 < (\bigodot_A.r + \bigodot_B.r)^2$. This inequality verifies the squared distance between two spheres, using the 3-vector Euclidean norm, $\| . \|_2$, and requires 11 basic operations.

The overlap test can be applied using the brute force or the BVH strategies. In the brute force strategy, every sphere is compared against the other spheres, and in the BVH strategy, a k-ary BVH is required to be constructed in the preprocessing stage to be traversed in this running stage. We proceeded to implement the former strategy due to the number of spheres handled is small.

Let $\zeta_j = \{\bigodot_0, \bigodot_1, ..., \bigodot_{n-1}\}$ be the set of spheres in chain j, n be the number of spheres per chain, and n_c be the number of chains. We can perform the collision detection process computing the overlap among all the spheres of the mesh. The collision detection can be computed in every chain independently of the other chains.

In the $\mathcal{M}_2$ approach (without chains) we consider the total number of spheres in the mesh m, thus m^2 comparisons for all the spheres are required. In the $\mathcal{M}_1$ approach (with chains), $\bigodot_i$ is compared against the other spheres. The algorithm requires $O(n)$ time for a sphere, that is $O(n^2)$ for a chain, and $O(n_c n^2)$ for all the chains, being n the number of spheres in each chain and n_c the number of chains.

The overlap test is considered for all the spheres of the torso. Left side spheres are considered in chains ζ_0 and ζ_5, right side spheres are considered in chains ζ_1 and ζ_4. Two spheres collide when they are not adjacent.

The parallelization of the methods $\mathcal{M}_1$, and $\mathcal{M}_2$ gives a change in the performance and exploits the features of each method. In the second method $\mathcal{M}_2$, we can have a thread per sphere, then we would have a $O(m)$ time (Figure 11). In the method $\mathcal{M}_1$, using chains, we can have n_c threads and the time expected is $O(n^2)$. On the other hand, increasing the number of threads by n^2, the time is reduced to $O(n)$ since the overlap test is performed per sphere in each chain.

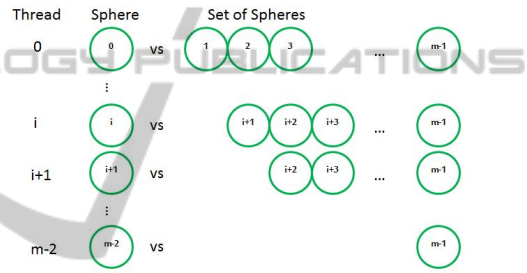

Figure 11: m threads are launched to perform the overlap test for each sphere.

6 EXPERIMENTS

Our experiments were run on a PC with a 2.40GHz Xeon processor, 12 GB main memory with Windows 7 operating system. The algorithm was coded in C++ with OpenGL API. We employed a human mesh. The human was constructed using the MakeHuman tool and has 26,292 polygons. Two kinds of experiments were carried on, firstly the sphere approximation of the pre-processing stage, and secondly the collision detection of the running stage.

The first experiment is based on the accuracy of the spheres created, comparing the method φ_1 with the minimum enclosing ball method φ_2. The accuracy of the spheres created can be tested by the distance measure F among the vertices of the surrounding region and the spheres that cover such region. The parameters considered are as follows: number of rays in the disk (N_r), number of spheres per level (N_s), displacement of the disk δ, and penetration depth PD. We take $N_r = 80$ and $\delta = 0.25$. Penetration depth

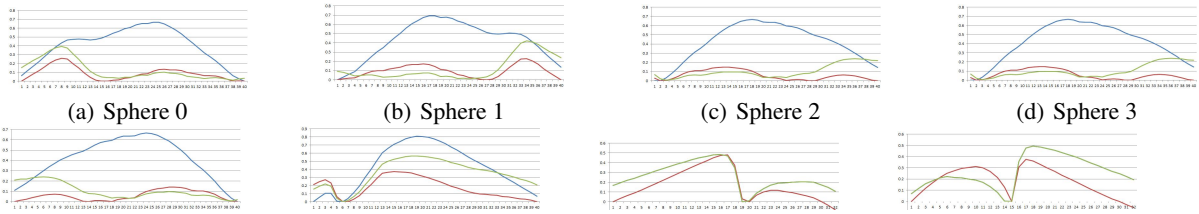

(a) Sphere 0 (b) Sphere 1 (c) Sphere 2 (d) Sphere 3

(e) Sphere 4 (f) Sphere 5 (g) Sphere 6 (h) Sphere 7

Figure 13: Approximation of the human with 2 spheres per level, using φ_1 (blue), φ_2 (red) and φ_1' (green).

refers to the overlapping spheres, that is $PD = 0$ if non-overlap exists, and 0.50 if the half of the two spheres involved are overlapped.

Our experiments were conducted to measure the accuracy of the spheres created. We employed $N_s = 2$, and $PD = 30\%$. We perform the calculus of the spheres by the first (φ_1) and the second (φ_2) methods, then we adjusted φ_1 to enhance the accuracy (φ_1') using the Sphere Adjustment routine. Spheres are labeled in a bottom-up manner, from left to right as shown in Figure 12. We name the rays of the disc as $r_0, r_1, \ldots, r_{79}$ and compare the rays length of the spheres for both methods φ_1' and φ_2.

In sphere 0, φ_2 is better in the first half of the set of the colliding points. On the contrary, in sphere 1, φ_1' is better in the first half of the set of the colliding points. In spheres 2 and 3 the behavior is the same as in spheres 0 and 1, respectively; this means that the torso shape remains equal. In sphere 4, φ_2 is better from r_8 and in sphere 5, φ_2 is better in r_0-r_{25}. In spheres 6 and 7, $\varphi_2 = \varphi_1'$ in the middle of the colliding points, and φ_1' is better before r_{16} for sphere 6 and after r_{16} for sphere 7 (Figure 13).

φ_1' has a better approximation than φ_2 in regions with non circular shape, otherwise φ_2 has a better approximation.

The second experiment consists of the collision detection in the running stage. The human is animated using 40 frames (Figure 14). The number of overlaps is bigger in $\mathcal{M}_1$ since the spheres are repeated in some chains. The average number of spheres in each chain is 23, then the 6 chains contain 138 spheres, more than the total number of spheres in the mesh: 80.

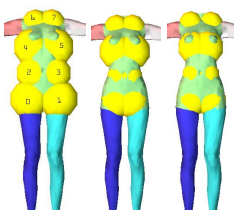

(a) φ_1 (b) φ_2 (c) φ_1'

Figure 12: Approximation of spheres 0, 1, 2, 3, 4 and 5 using 2 spheres per level.

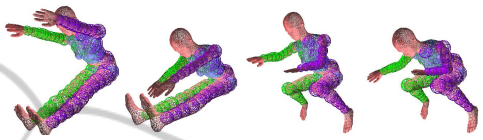

Figure 14: The human animation.

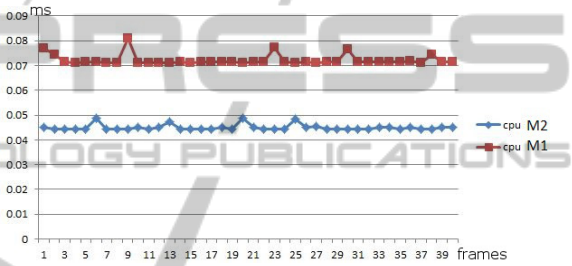

Figure 15: The time in milliseconds of the the running stage of methods $\mathcal{M}_1$ and $\mathcal{M}_2$ using CPU.

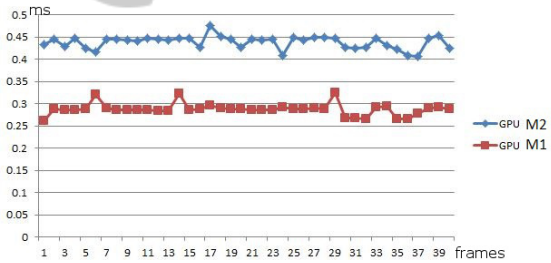

Figure 16: The time in milliseconds of the the running stage of methods $\mathcal{M}_1$ and $\mathcal{M}_2$ using GPU.

Figure 15 shows the time in milliseconds for evey frame, comparing the methods $\mathcal{M}_1$ (chains) and $\mathcal{M}_2$ (no chains) in CPU. $\mathcal{M}_2$ is faster than $\mathcal{M}_1$ as the number of tests is smaller. In the GPU, $\mathcal{M}_1$ takes less time than $\mathcal{M}_2$ as illustrated in Figure 16. This is because the parallel run when using threads. In both cases CPU and GPU, the number of overlaps is bigger in $\mathcal{M}_1$ than in $\mathcal{M}_2$. CUDA was employed to parallelize the algorithm.

Since we are handling few spheres, the parallelism is not exploiting, we require much more spheres as indicated in (Enrique Ayala, 2014) about 10,000 or more. To overcome this problem a hierarchy should be done, creating children and parent nodes from the current spheres. Additionally, we could consider

more humans moving around, and then perform both, the self-collision detection in each human, and the collision detection between pairs of humans.

Observe that the number of spheres per chain indicates the number of overlapping tests, independent of the animation employed. This occurs because of the self-collision process in a chain. We proved this statement by running a second animation, obtaining similar times.

7 CONCLUSIONS

A collision detection algorithm is detailed that employs sphere chains as a preprocessing stage. Our method is performed for the broad phase collision detection and can be used in articulated objects where tubular regions are presented. We take into account the surrounding regions which can be returned when spheres are colliding. For more accuracy, a narrow phase algorithm should be employed.

Our limitations are as follows: more chains are required to exploit the parallel implementation, head, hands, and feet are not considered.

The work can be extended by computing the collision detection in several humans, using of a BVH (binary, quadtree, octree, hybrid), using other types of BVs, utilizing other objects: human hand, snakes, animals with several legs such as octopus, spider, quadrupeds. The sphere refitting can achieve more accuracy by considering more pivot polygons.

We could extent our approach to Continuous Collision Detection by implementing an interpolation between the human motion trying to avoid the tunneling problem and other parallel techniques can be applied.

ACKNOWLEDGEMENTS

I want to thank to CONACYT and the University of Yucatan for their financial support.

REFERENCES

Enrique Ayala, Francisco A. Madera, F. M.-M. (2014). Self-collision detection in tubular objects approximated by spheres. *IJCSI International Journal of Computer Science Issues*, 11(5):14–21.

Ericson, C. (2005). *Real-Time Collision Detection*. Morgan Kaufmann publishers.

Guibas, L., Nguyen, A., Zhang, L., and Russel, D. (2002). Collision detection for deforming necklaces. In *In Symposium on Computational Geometry*, pages 33–42.

Kavan, L., O'Sullivan, C., and Žára, J. (2006). Efficient collision detection for spherical blend skinning. In *Proceedings of the 4th International Conference on Computer Graphics and Interactive Techniques in Australasia and Southeast Asia*, GRAPHITE '06, pages 147–156, New York, NY, USA. ACM.

Kim, Y. J., Manocha, D., and Tang, M. (2014). Hierarchical and controlled advancement for continuous collision detection of rigid and articulated models. *IEEE Transactions on Visualization and Computer Graphics*, 20(5):755–766.

Li, J., Lu, G., and Ye, J. (2011). Automatic skinning and animation of skeletal models. *Vis. Comput.*, 27(6-8):585–594.

Madera, F. A., Laycock, S. D., and Herrera, C. G. (2013). Ray-triangle collision detection to approximate objects with spheres. In *Proceedings of the IASTED International Conference on Computer Graphics and Imaging, CGIM 2013*, pages 70–76.

Müller, M. and Chentanez, N. (2011). Adding physics to animated characters with oriented particles. In Bender, J., Erleben, K., and Galin, E., editors, *VRIPHYS*, pages 83–91. Eurographics Association.

Shier, J. and Bourke, P. (2013). An algorithm for random fractal filling of space. *Computer Graphics Forum*, 32(8):89–97.

Teuber, J., Weller, R., Zachmann, G., and Guthe, S. (2013). Fast sphere packing with adaptive grids on the gpu. In Brunnett, G., Coquillart, S., and Welch, G., editors, *In GI AR VRWorkshop*, pages 181–201, Würzburg, Germany. Springer Vienna.

Wang, P., Lau, R. W., Pan, Z., Wang, J., and Song, H. (2014). An eigen-based motion retrieval method for real-time animation. *Computers & Graphics*, 38(0):255 – 267.

Weller, R. and Zachmann, G. (2009). Technical Report lfl-09-09, Department of Informatics, Clausthal University of Technology, Clausthal-Zellerfeld, Germany.

Welzl, E. (1991). Smallest enclosing disks (balls and ellipsoids). In *Results and New Trends in Computer Science*, pages 359–370. Springer-Verlag.

Zhang, X., Redon, S., Lee, M., and Kim, Y. J. (2007). Continuous collision detection for articulated models using taylor models and temporal culling. *ACM Trans. Graph.*, 26(3).

Zhu, S., Mok, P. Y., and Kwok, Y. L. (2013). An efficient human model customization method based on orthogonal-view monocular photos. *Comput. Aided Des.*, 45(11):1314–1332.